



University Medical Center Groningen

University of Groningen

## Photophysical and electronic properties of bismuth-perovskite shelled lead sulfide quantum dots

Abdu-Aguye, Mustapha; Bederak, Dmytro; Kahmann, Simon; Killilea, Niall; Sytnyk, Mykhailo; Heiss, Wolfgang; Loi, Maria Antonietta

*Published in:*  
Journal of Chemical Physics

*DOI:*  
[10.1063/1.5128885](https://doi.org/10.1063/1.5128885)

**IMPORTANT NOTE: You are advised to consult the publisher's version (publisher's PDF) if you wish to cite from it. Please check the document version below.**

*Document Version*  
Publisher's PDF, also known as Version of record

*Publication date:*  
2019

[Link to publication in University of Groningen/UMCG research database](#)

### *Citation for published version (APA):*

Abdu-Aguye, M., Bederak, D., Kahmann, S., Killilea, N., Sytnyk, M., Heiss, W., & Loi, M. A. (2019). Photophysical and electronic properties of bismuth-perovskite shelled lead sulfide quantum dots. *Journal of Chemical Physics*, 151(21), [214702]. <https://doi.org/10.1063/1.5128885>

### **Copyright**

Other than for strictly personal use, it is not permitted to download or to forward/distribute the text or part of it without the consent of the author(s) and/or copyright holder(s), unless the work is under an open content license (like Creative Commons).

### **Take-down policy**

If you believe that this document breaches copyright please contact us providing details, and we will remove access to the work immediately and investigate your claim.

*Downloaded from the University of Groningen/UMCG research database (Pure): <http://www.rug.nl/research/portal>. For technical reasons the number of authors shown on this cover page is limited to 10 maximum.*

# Photophysical and electronic properties of bismuth-perovskite shelled lead sulfide quantum dots

Cite as: J. Chem. Phys. **151**, 214702 (2019); <https://doi.org/10.1063/1.5128885>

Submitted: 24 September 2019 . Accepted: 12 November 2019 . Published Online: 02 December 2019

Mustapha Abdu-Aguye , Dmytro Bederak , Simon Kahmann , Niall Killilea, Mykhailo Sytnyk, Wolfgang Heiss , and Maria Antonietta Loi 

## COLLECTIONS

Paper published as part of the special topic on [Colloidal Quantum Dots](#)

Note: This paper is part of the JCP Special Topic on Colloidal Quantum Dots.



View Online



Export Citation



CrossMark

## ARTICLES YOU MAY BE INTERESTED IN

[Properties of quantum dots coupled to plasmons and optical cavities](#)

The Journal of Chemical Physics **151**, 210901 (2019); <https://doi.org/10.1063/1.5124392>

[Coherent charge-phonon correlations and exciton dynamics in orthorhombic  \$\text{CH}\_3\text{NH}\_3\text{PbI}\_3\$  measured by ultrafast multi-THz spectroscopy](#)

The Journal of Chemical Physics **151**, 214201 (2019); <https://doi.org/10.1063/1.5127992>

[Composition effect on the carrier dynamics and catalytic performance of  \$\text{CuInS}\_2/\text{ZnS}\$  quantum dots for light driven hydrogen generation](#)

The Journal of Chemical Physics **151**, 214705 (2019); <https://doi.org/10.1063/1.5125024>



Lock-in Amplifiers

Zurich Instruments

Watch the Video

# Photophysical and electronic properties of bismuth-perovskite shelled lead sulfide quantum dots

Cite as: J. Chem. Phys. 151, 214702 (2019); doi: 10.1063/1.5128885

Submitted: 24 September 2019 • Accepted: 12 November 2019 •

Published Online: 2 December 2019



View Online



Export Citation



CrossMark

Mustapha Abdu-Aguye,<sup>1</sup>  Dmytro Bederak,<sup>1</sup>  Simon Kahmann,<sup>1</sup>  Niall Killilea,<sup>2</sup> Mykhailo Sytnyk,<sup>2</sup> Wolfgang Heiss,<sup>2</sup>  and Maria Antonietta Loi<sup>1,a)</sup> 

## AFFILIATIONS

<sup>1</sup>Photophysics and Optoelectronics, Zernike Institute for Advanced Materials, University of Groningen, Nijenborgh 4, 9747AG Groningen, The Netherlands

<sup>2</sup>Department of Materials Science and Engineering, Institute of Materials for Electronics and Energy Technology, Friedrich-Alexander-Universität Erlangen-Nürnberg, Energy Campus Nürnberg, 90429 Nürnberg, Germany

**Note:** This paper is part of the JCP Special Topic on Colloidal Quantum Dots.

<sup>a)</sup>Author to whom correspondence should be addressed: [m.a.loi@rug.nl](mailto:m.a.loi@rug.nl)

## ABSTRACT

Metal halide perovskite shelled quantum dot solids have recently emerged as an interesting class of solution-processable materials that possess the desirable electronic properties of both quantum dots and perovskites. Recent reports have shown that lead sulfide quantum dots (PbS QDs) with perovskite ligand-shells can be successfully utilized in (opto)electronic devices such as solar cells, photoconductors, and field-effect transistors (FETs), a development attributed to the compatibility of lattice parameters between PbS and certain metal halide perovskites that results in the growth of the perovskite shell on the PbS QDs. Of several possible perovskite combinations used with PbS QDs, bismuth-based variants have been shown to have the lowest lattice mismatch and to display excellent performance in photoconductors. However, they also display photoluminescence (PL), which is highly sensitive to surface defects. In this work, we present an investigation of the transport and optical properties of two types of bismuth-based perovskite ( $\text{MA}_3\text{BiI}_6$  and  $\text{MA}_3\text{Bi}_2\text{I}_9$ ) shelled PbS QDs. Our photophysical study using temperature-dependent PL spectroscopy between 5 and 290 K indicates that the PL efficiency of the reference oleic acid (OA) capped samples is much higher than that of the Bi-shelled ones, which suffer from traps, most likely formed at their surfaces during the phase-transfer ligand exchange process. Nevertheless, the results from electrical measurements on FETs show the successful removal of the native-OA ligands, displaying electron dominated transport with modest mobilities of around  $10^{-3} \text{ cm}^2 [\text{V s}]^{-1}$  – comparable to the reported values for epitaxial Pb-based shelled samples. These findings advance our understanding of perovskite shelled QD-solids and point to the utility of these Bi-based variants as contenders for photovoltaic and other optoelectronic applications.

Published under license by AIP Publishing. <https://doi.org/10.1063/1.5128885>

## INTRODUCTION

Colloidal nanocrystals, or quantum dots (QDs), have attracted much attention over the past two decades for several important technological applications in fields as diverse as biological imaging,<sup>1</sup> drug delivery,<sup>2</sup> energy conversion<sup>3,4</sup> and storage,<sup>5</sup> and optoelectronics. For optoelectronic applications, their potential is mostly determined by the quantum-size effect that allows for tuning the bandgap<sup>6</sup>

(and therefore absorption and emission) from the ultraviolet to the near-infrared spectral region as well as the ability to be processed through simple solution-based deposition methods for cost-effective and scalable mass production. Furthermore, they often exhibit superior stability compared to other solution-processable optoelectronic materials.<sup>7</sup> Among the many combinations of materials for QD-based optoelectronic devices, lead chalcogenides (PbX, X = S, Se, and Te) are some of the most common due to their well-developed

synthetic process, good carrier mobilities, and their photosensitivity in the (near) infrared region coupled to a relatively large exciton Bohr radius (~18, 46, and 150 nm for PbS, PbSe, and PbTe, respectively), which enables them to retain quantum confinement even in relatively large particle sizes.<sup>8</sup>

Decades of research into QD-based optoelectronics have led to great improvements in the synthetic techniques and to enhanced material quality, tuning of the electronic properties via surface modification or ligand exchange, and control of the formation of QD solids via a host of deposition techniques such as spin-coating, blade-coating, or spray-coating. Surface ligands are necessary additives during synthesis of colloidal QDs to stop growth and impart solubility, thus aiding in long-term colloidal stability. However, these ligands are generally rather long and create a large potential barrier. Therefore, when charge carriers need to be extracted, ligand exchange should be carried out to replace the native long insulating ligands such as oleic acid (OA) with shorter ones in order to improve the electronic coupling between adjacent QDs.<sup>9</sup> The first generation of QD-based optoelectronic devices such as electrochemical cells, field effect transistors (FET), solar cells, and photodetectors<sup>10–13</sup> featured postdeposition (or solid state) ligand exchange with short (bidentate) molecules such as thiols [ethanedithiol (EDT), 3-mercaptopropionic acid (MPA)], amines [butylamine (BA)], metal thiocyanates, etc. However, rather great challenges, related to film shrinkage, and the torturous layer-by-layer (LbL) processing to obtain films of the desired thickness appeared very soon.

Recently, solution-based ligand exchange methods such as liquid phase transfer where the ligand dissolved in a polar solvent reacts with the surface of the QDs, leaving the pristine ligand behind in the nonpolar phase and bringing the QDs to the polar phase, have been reported by several groups.<sup>9,11,14–16</sup> These inks are desirable because a single deposition step can be used to obtain films of the desired thickness, and also these layers appear less prone to form cracks during solvent evaporation.<sup>17,18</sup> Ligands such as metal chalcogenide complexes, thiols, (pseudo)halides, metal halides, and more recently (hybrid) metal halide (ABX<sub>3</sub>) ligands<sup>19</sup> have been reported. Besides their chemical compatibility with the surface of Pb chalcogenides, the rise of metal halide ligands is linked partially to their excellent optical and electronic properties as standalone materials, and also several studies have shown a good lattice match with chalcogenide QD materials, such as PbS.<sup>20</sup> Pb-based perovskites have been the most widely studied ligands, but also other metal ion complexes based on Sn<sup>2+</sup>, Mn<sup>2+</sup>,<sup>21</sup> In<sup>3+</sup>,<sup>22</sup> and Bi<sup>3+</sup><sup>23,24</sup> have recently been studied as alternatives. Bi, in particular, has been recently reported as a metal ion that can be used to form an interesting perovskite and perovskitelike materials.<sup>25–29</sup>

Recently, Sytnyk and co-workers reported the preparation and characterization of high-quality perovskite shelled PbS QDs featuring high carrier mobility, and excellent results in photoconductor applications. Their experiments on octahedral metal halide clusters: (MA<sup>+</sup>)<sub>(6-x)</sub> [M<sup>(x+)</sup> Hal<sub>6</sub>]<sup>(6-x)-</sup> with (MA = methylammonium, M<sup>x+</sup> = Pb<sup>2+</sup>, Bi<sup>3+</sup>, Mn<sup>2+</sup>, In<sup>3+</sup>, and Hal = Cl, I) resulted in MA<sub>3</sub>BiI<sub>6</sub> coated PbS based devices showing the best performance—an observation they attributed to the low lattice mismatch of ca. -1%, which resulted in the most efficient passivation of the PbS core. Interestingly, this same Bi-based ligand shelled QD displayed a full quenching of the photoluminescence (PL) when in solution, which was interpreted as

due to the formation of a staggered heterostructure between the PbS core and the (BiI<sub>6</sub>)<sup>-3</sup> clusters.<sup>30</sup> This is in contrast with what has been reported for Pb-based perovskite shelled QDs, which display similar PL (peak position and lifetimes) to OA-capped QDs in solution.<sup>18</sup> In addition, the PbS inks using (PbI<sub>3</sub>)<sup>-</sup> as a ligand have shown very good performance as active materials in solar cells and field effect transistors.<sup>15,18,31,32</sup> For this reason, the surprising behavior of the Bi-based PbS QD ligand warrants further investigation.

In this study, two Bi-shelled PbS QD inks were synthesized using a modified procedure reported by Sytnyk *et al.*<sup>30</sup> These are expected to have compositions of MA<sub>3</sub>BiI<sub>6</sub> and MA<sub>3</sub>Bi<sub>2</sub>I<sub>9</sub>, the former was also studied by Sytnyk and co-workers, while the latter was not reported earlier as a PbS ligand although the MA<sub>3</sub>Bi<sub>2</sub>I<sub>9</sub> Perovskite was used as an active layer for solar cells<sup>33</sup> and as a light emitter.<sup>34</sup>

## EXPERIMENTAL

### Ink preparation

PbS QDs were synthesized in a similar manner to that reported elsewhere.<sup>35</sup> Solution-state ligand exchange was performed by using a modified recipe from Sytnyk *et al.*<sup>30</sup> In a typical procedure, 50 mM ligand solution in 10 ml DMF was prepared by mixing MAI and BiI<sub>3</sub> in a 3:1 ratio for MA<sub>3</sub>BiI<sub>6</sub>, or in a 3:2 ratio for MA<sub>3</sub>Bi<sub>2</sub>I<sub>9</sub>. In both cases, the ligand solution turns red upon stirring and heating at 100 °C on a hot-plate. After cooling, the ligand solution was mixed with 10 ml of hexane dispersion of oleate-capped PbS CQDs with a concentration of about 5 mg/ml. The mixture was stirred until the CQDs transformed into the polar phase. Then, the top phase was discarded and the polar phase was washed 3 times with 10 ml of hexane. The Bi-shelled PbS CQDs were then precipitated by the addition of toluene and collected by centrifugation. The supernatant was removed, and the CQDs were redispersed in either 2,6-difluoropyridine (DFP) or propylene carbonate (PC) to form a QD ink.

### Absorption spectroscopy

Absorption measurements were carried out on dilute inks in 2 mm path length quartz cuvettes or on masked areas of thin films deposited by spin-coating on quartz substrates using a dual beam Shimadzu spectrophotometer (UV-3600). From the absorption peak position of the OA-capped PbS QDs (~849 nm), we estimate a particle size of approximately 2.7 nm.<sup>36</sup>

### Photoluminescence (PL) spectroscopy

PL measurements were carried out by exciting (unwashed) blade-coated samples with the 2nd harmonic of a Ti:sapphire resonator ( $\lambda \approx 400$  nm). Measurements were carried out in the transmission mode, and the spectra were collected using a monochromator with 30 lines/mm and were recorded using an ANDOR InGaAs inline detector (iDUS-1700). The laser spot on the sample was focussed via a 15 cm focal length lens, resulting in a diameter of approximately 100  $\mu$ m.

For power dependent measurements, a neutral density filter wheel was used to vary the excitation power on the sample; for temperature dependent measurements, a cryostat equipped with

flow and temperature controllers (Oxford Instruments) was used with liquid helium. All the recorded spectra were corrected for the response of the setup using a calibrated lamp.

### Field effect transistor (FET) fabrication and measurement

The substrates for FETs consist of highly doped Si with thermally grown 230 nm  $\text{SiO}_2$  as a gate dielectric. Prepatterned ITO/Au electrodes served as a source and a drain electrode and formed a channel of 1 cm width and 20  $\mu\text{m}$  length. The substrates were cleaned by consecutive sonication in acetone and isopropanol, dried in an oven, and treated by oxygen-plasma for 3 min before QD film deposition. The QD films were deposited by spin coating the ink of ligand-exchanged QDs in 2,6-difluoropyridine (DFP) at 1000 rpm after which the films were washed with methanol. The films were annealed for 20 min at 120 °C after the fabrication and then

analyzed using an Agilent E5262 semiconductor parameter analyzer. All transistor fabrication and measurements were performed in a nitrogen-filled glovebox.

### RESULTS AND DISCUSSION

Figure 1(a) shows a schematic representation of the phase-transfer ligand exchange process employed to make the inks, as well as the layouts of samples for PL spectroscopy and FET measurements. Figures 1(b) and 1(c) show the absorption spectra of the Bi-based inks (in DFP) and thin films. We note that the Bi-based inks display a weaker excitonic peak compared to the OA-based reference sample. This (inhomogeneous) broadening of the excitonic peak is likely due to the changes in the surface passivation upon OA removal; furthermore, the variation of the solvent and consequently of its polarity (DFP has a dielectric constant of 107.8) can also explain this effect, as it has been observed by other

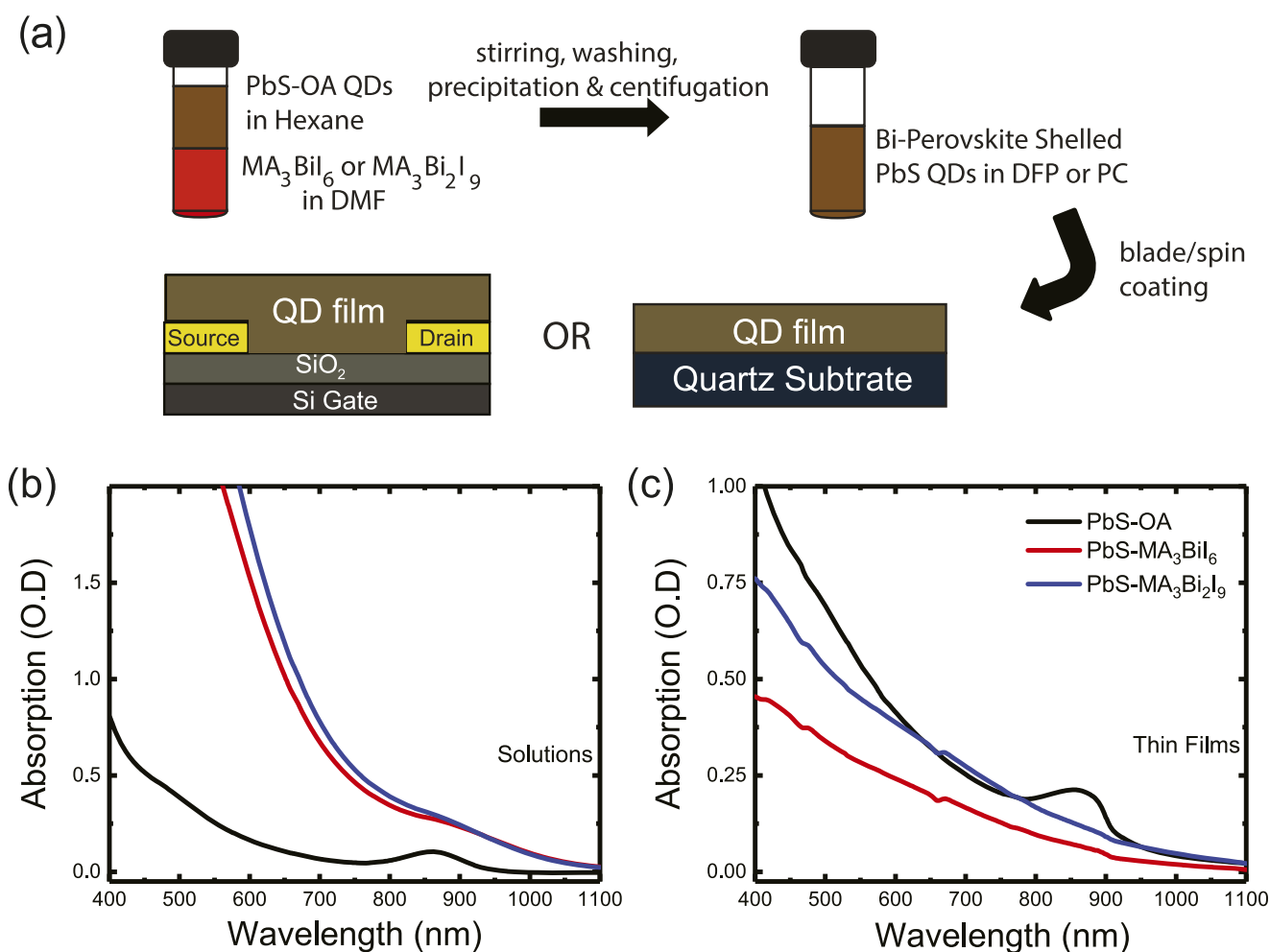


**FIG. 1.** (a) Scheme of the phase transfer ligand exchange process. (b) Absorption spectra of the OA-capped PbS QD solution (in hexane) and Bi perovskite shelled PbS QDs in DFP. (c) Corresponding spectra of thin films on quartz substrates.

authors.<sup>18,37</sup> When thin films of the QDs are cast onto quartz substrates, once again, the Bi-based samples do not display a clear excitonic peak, unlike the OA-based sample. In this case, the absence of the excitonic peak is expected to result from a changed dielectric environment and closer electronic coupling between adjacent QDs.<sup>18,38</sup>

The photoluminescence spectra of the inks are shown in Fig. 2(a). The Bi-perovskite shelled inks display broad peaks along with a tail at longer wavelengths, and such broad spectra in solution are peculiar, in particular, when compared with the parent OA-based sample that displays a narrow peak at 995 nm without any sub-bandgap emission or signs of extensive polydispersity. The dips in the solution PL spectra at  $\sim 1035$  nm are due to the absorption of the (relatively weak) PL from the QDs by the solvent (DFP). While broad PL spectra have been reported for several ligands such as TBAI, EDT,

and MPA,<sup>39–41</sup> these apply to thin films and not to inks or solutions. These broad low energy features in the Bi-based samples seem to indicate clustering of the QDs driven by excess ligands. When cast into films via blade coating, the PL peaks for both Bi-based samples resemble the OA-based reference sample very closely [see Fig. 2(b)]; with an approximately 20 nm redshift relative to their main peaks in solution, it should be noted that the films are unwashed. This leads to the question: What determines the large variation in the shape of the Bi-shelled samples?

To gain more information about the electronic properties of the Bi-perovskite shelled QDs, field effect transistors were fabricated on Si/SiO<sub>2</sub> substrates, and the output characteristics are shown in Figs. 2(c) and 2(d). The extracted linear mobility values ( $1.4 \times 10^{-3}$  and  $1.4 \times 10^{-3}$  cm<sup>2</sup> [V s]<sup>-1</sup> for the MA<sub>3</sub>BiI<sub>6</sub> and MA<sub>3</sub>Bi<sub>2</sub>I<sub>9</sub>-shelled QDs, respectively), although lower than recent records for LbL PbS

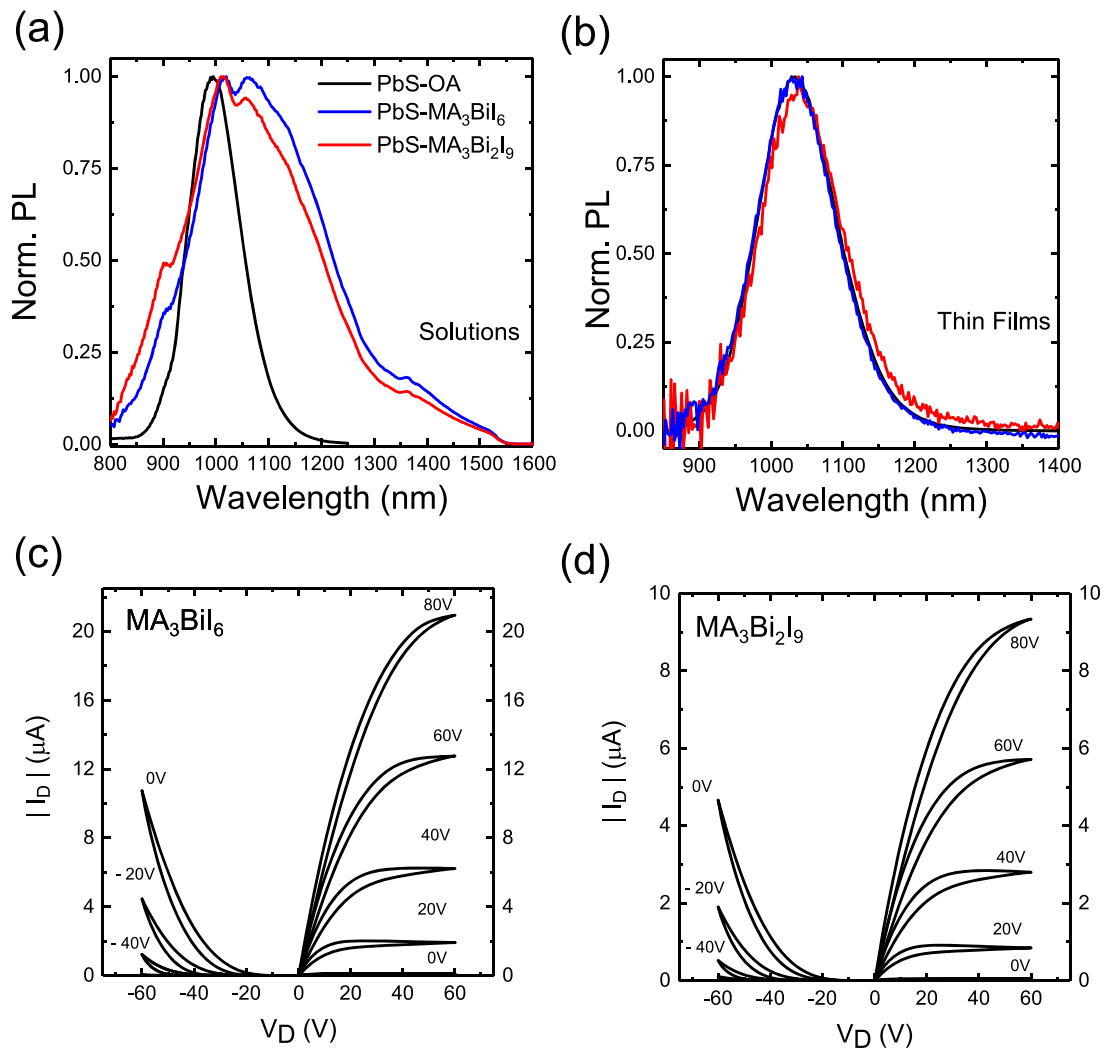


**FIG. 2.** Steady-state photoluminescence spectra of OA-capped and Bi-perovskite shelled PbS QD solution/inks (a) and thin films on quartz—note that the spectra of PbS-OA and PbS-MA<sub>3</sub>BiI<sub>6</sub> are superposed (b); output curves of field effect transistors based on (c) MA<sub>3</sub>BiI<sub>6</sub> and (d) MA<sub>3</sub>Bi<sub>2</sub>I<sub>9</sub> shelled QDs.

QD FETs,<sup>42</sup> are encouraging first results for Bi-perovskite shelled PbS-QD thin films, and compare favorably with mobilities of other PbS inks, such as those with ligands such as MAPbI<sub>3</sub>, MPA, and halides.<sup>18,43,44</sup> More importantly, these results confirm the removal of the native OA based ligands without which transport is essentially impossible.<sup>45,46</sup> As can be seen by the higher drain currents in the n-channel from the output curves, the FETs display more electron-dominant transport. This is also reflected in the transfer curves depicted in Fig. S1.

Temperature-dependent PL measurements are an important tool to gauge more physical information about QD solids. Figure 3(a) shows the strong temperature dependence of the PL from reference thin films of OA-capped QDs. The PL at room temperature (RT) exhibits a single peak at ~1040 nm with a FWHM of 123 nm. When the temperature is decreased, the PL emission becomes stronger, as has been variously reported before in PbX QDs.<sup>47,48</sup> At 5 K, it is already more than double in intensity and the FWHM has decreased to ~91 nm. Another consequence of

decreasing the temperature is a bathochromic shift of the emission from RT to 5 K (1040 nm–1069 nm). This red shifted PL emission can be explained as an interplay between the thermal expansion of the QDs described by a size-dependent temperature coefficient and temperature-mediated interactions between phonons and charge carriers as well as the effect of confinement energy on the effective masses of carriers.<sup>48,49</sup> The increasing PL intensity and decreasing FWHM at low temperature are a consequence of reduced electron-phonon scattering due to the reduced number of lattice vibrations at low temperature, which is known to result in quenching of excitons.<sup>38</sup> The evolution of the FWHM and peak position as a function of temperature are shown in Figs. 4(a) and 4(b).

For the Bi-perovskite capped PbS QD films, the temperature dependent PL spectra are shown in Figs. 3(b) and 3(c) - with RT peak positions at 1042 nm and 1037 nm for the [BiI<sub>6</sub>]<sup>3-</sup> and [Bi<sub>2</sub>I<sub>9</sub>]<sup>3-</sup> samples, respectively; and FWHM values of 127 nm and 123 nm. Similar to the OA-based reference sample, there is

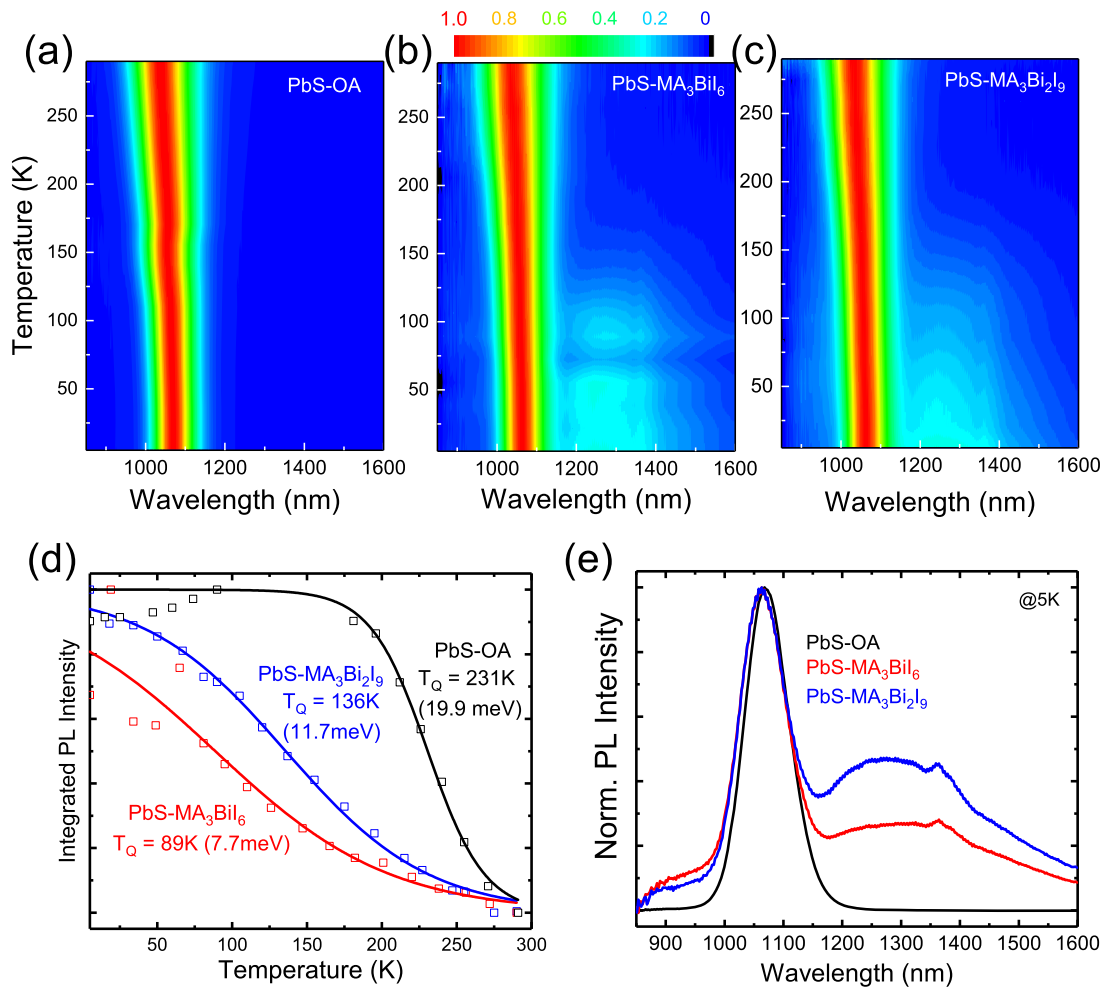


**FIG. 3.** Temperature dependent PL plots of (a) OA-capped PbS QDs, (b) PbS-MA<sub>3</sub>BiI<sub>6</sub> QDs, and (c) PbS-MA<sub>3</sub>Bi<sub>2</sub>I<sub>9</sub> QDs. (d) Integrated PL intensity vs temperature plots of the OA and Bi-shelled PbS QDs fit to Eq. (1) with obtained values for the quenching temperature,  $T_Q$  and (e) representative PL spectra of the samples at 5 K.

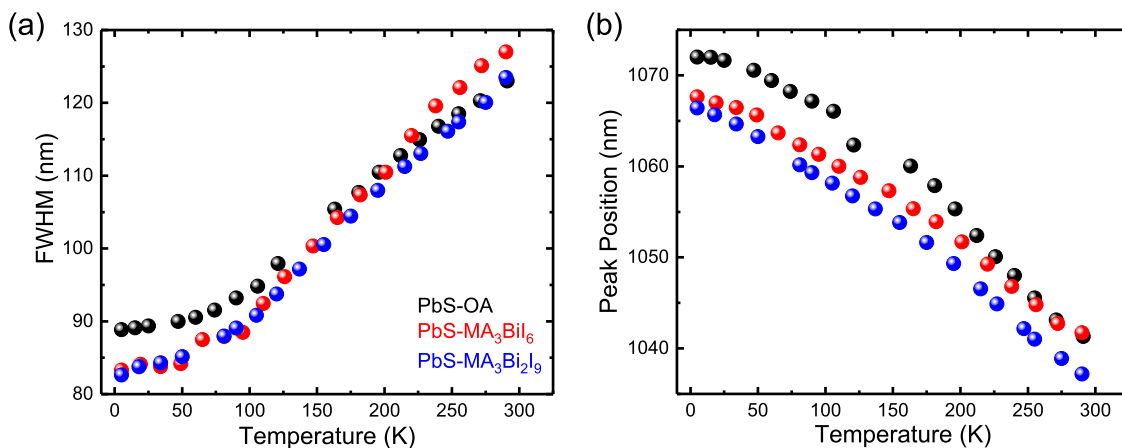


FIG. 4. The (a) FWHM and (b) peak position of the PL emission as a function of temperature for the PbS-OA, PbS-MA<sub>3</sub>BiI<sub>6</sub>, and PbS-MA<sub>3</sub>Bi<sub>2</sub>I<sub>9</sub> samples.

a bathochromic shift of the PL as temperature decreases together with a corresponding increase in the PL intensity (by a factor of  $\sim 5$  between RT and 5 K in both cases), i.e., a quenched PL is obtained as temperature goes up from 5 K. Temperature-mediated PL quenching is usually quantified in terms of a Boltzmann model,<sup>50</sup>

$$I_{PL}(T) = \frac{1}{1 + \exp[(T - T_Q)/\varphi]}, \quad (1)$$

where  $I_{PL}$  is the integrated PL intensity (normalized, in this case);  $T_Q$  and  $\varphi$  are fit parameters representing the quenching temperature and rate, respectively.  $T_Q$  can be interpreted as the temperature associated with thermal quenching of excitons, and  $\varphi$  represents a quenching rate associated with  $T_Q$ . In general, a higher  $T_Q$  is necessary for better stabilization of excitons and more efficient PL.<sup>26</sup> From the fits shown in Fig. 3(d), we obtain  $T_Q$  values of 89 K, 136 K, and 231 K, corresponding to thermal energies (required for the nonradiative quenching of excitons) (i.e.,  $k_B T_Q$ ) of 7.7 meV, 11.7 meV, and 19.9 meV for the [BiI<sub>6</sub>]<sup>3-</sup>, [Bi<sub>2</sub>I<sub>9</sub>]<sup>3-</sup>, and OA capped samples, respectively. Figure 3(d) shows a comparison between the shapes of the PL of the samples at 5 K, as can be inferred from Figs. 3(b) and 3(c), the Bi-capped samples display a broad emission feature at lower energies in addition to the main peak. This behavior is all the more interesting since the same batch of OA-capped PbS QDs display very different behavior when Pb-based perovskite ligands (MAPbI<sub>3</sub> and MA<sub>4</sub>PbI<sub>6</sub>) are used [see Fig. S2 for their corresponding temperature-dependent PL spectra in contrast with Figs. 3(a)–3(c)].

This important feature of the temperature dependent PL spectra of the Bi-perovskite capped thin films initially emerges below approximately 100 K. A similar behavior has been observed in both thiol- (EDT, MPA) and I<sup>-</sup>-capped PbS QDs, and is attributed to radiative recombination from shallow below bandgap trap states.<sup>40,50,51</sup> Such an emission is absent in the reference OA-capped QD film, presumably because it passivates the QDs efficiently;<sup>52</sup> this can be seen from the PL shape, which remains unchanged at both 5 K and RT [see the supplementary material, Figs. S3(a)–S3(c)].

This indicates that the source of the trap states is the surface of the QDs. Furthermore, we can infer that these traps are induced by the ligand exchange process<sup>52,53</sup> and that the Bi-shelled QDs are not well passivated.

Turning our attention to the Bi-based PbS QD films, we performed power dependent PL measurements at both RT and 5 K. The Bi-perovskite shelled samples display changing spectra as a function of excitation power, showing a trap-filling mechanism occurring at these temperatures as the excitation power is increased [see Figs. S4(c)–S4(f)]. Figure 5 shows a plot of the integrated PL intensity vs the excitation power density for the three samples both at room and low temperature. The slope of the measured data is the fit to a power law relation of the form<sup>54</sup>

$$I_{PL}(P) = \eta P^\alpha, \quad (2)$$

where  $I_{PL}$ ,  $P$ , and  $\alpha$  represent the integrated PL intensity, excitation power density, and a recombination exponent, respectively.  $\eta$  represents an empirical “catch all” term, which encompasses the PL quantum yield, absorption, sample geometry, etc. The recombination exponent,  $\alpha$ , is generally expected to fall between 1 for excitonic recombination and 2 for bimolecular recombination between uncorrelated electron-hole pairs.

It is important to note that the excitation power density of the Bi-shelled samples is over two orders of magnitude higher than that of the OA-capped one. Much higher PL signals from the reference OA-capped sample were obtained, which is further evidence for the lower amount of nonradiative recombination sites in the well passivated OA-sample. An additional important consideration is that the occurrence of energy transfer has been reported in the case of OA-capped QDs.<sup>49</sup> Thus, in QDs with shorter ligands, energy transfer is expected to be more effective, increasing the probability of nonradiative recombination.

As mentioned earlier, the solid lines in the plots shown in Fig. 5 represent the best-fit to Eq. (2). As expected,  $\alpha$  of the OA-reference sample is approximately 1 at both 5 K and RT, and the  $\eta$  values remain very similar (5.52 and 5.20, respectively) at both temperatures, indicating a predominantly excitonic recombination



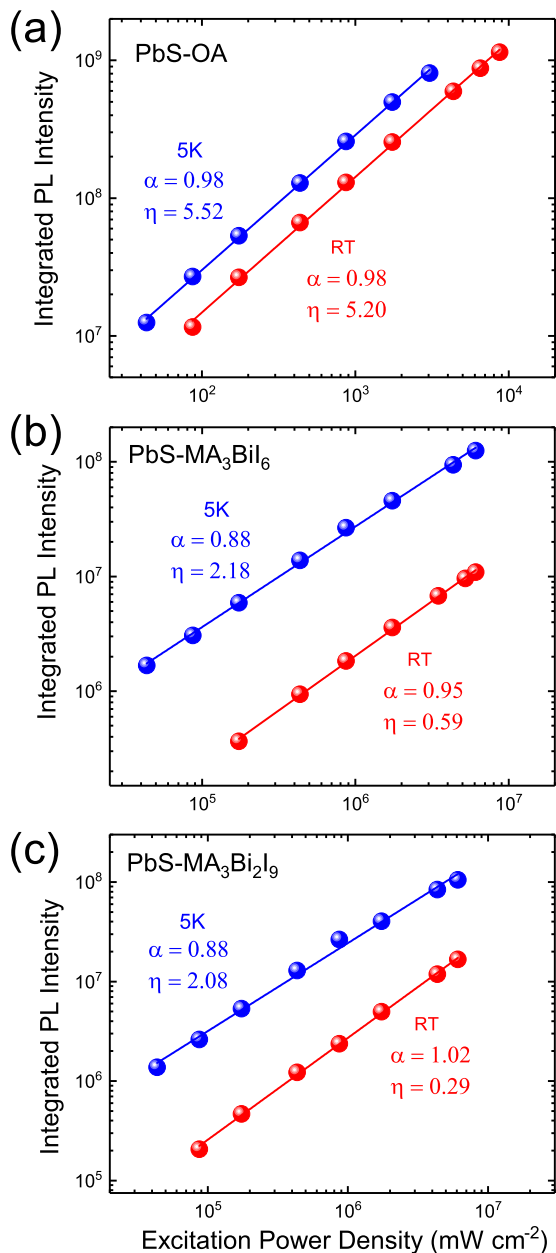


**FIG. 5.** Integrated PL vs excitation power density at 5 K and RT for (a) PbS-OA QDs, (b) PbS-MA<sub>3</sub>BiI<sub>6</sub> QDs, and (c) PbS-MA<sub>3</sub>Bi<sub>2</sub>I<sub>9</sub> QDs; insets show the extracted values for  $\alpha$  and  $\eta$  from Eq. (2).

mechanism with a slightly increased PL efficiency at 5 K compared to RT. For the Bi-based samples, on the other hand, a few interesting differences can be seen: the first is that although the recombination mechanism remains excitonic in nature ( $\alpha$  around 1), at 5 K it is lower (0.88 in both cases) than that at RT (0.95 and 1.02 for [BiI<sub>6</sub>]<sup>3-</sup> and [Bi<sub>2</sub>I<sub>9</sub>]<sup>3-</sup>, respectively).

This is in good agreement with the earlier observations of the emergence of a broad emission feature below the bandgap at low temperatures, which leads us to conclude that such below gap radiative states are indeed traplike. At RT, such PL signals are absent, which reflects in a higher  $\alpha$  value since the low temperature emission represents a loss mechanism to the mean excitonic emission peak. The second observation that can be made is that the  $\eta$  parameter varies significantly between RT and 5 K for both the [BiI<sub>6</sub>]<sup>3-</sup> sample (0.59 and 2.18 at RT and 5 K, respectively) and [Bi<sub>2</sub>I<sub>9</sub>]<sup>3-</sup> (0.29 and 2.08 at RT and 5 K). This large difference ( $\eta$  is on a log scale; thus, a difference of  $\Delta\eta = 1$  represents an order of magnitude difference in PL efficiency, under the assumption that all changes are temperature dependent) strongly shows that the PL efficiency of the Bi-based samples is much lower than that of the OA-based reference films, especially at RT.

A similar sublinear power dependence ( $\alpha < 1$ ) of the integrated PL of ligand-exchanged PbS films at low temperatures was reported before,<sup>50,51</sup> such observations, together with the assertion of an increased carrier lifetime at low temperatures reported before for both PbS<sup>55</sup> and PbSe<sup>47</sup> QDs, point toward either a redistribution of the excited state population from bright (highly radiative) exciton states to dark (relatively lower radiative) states or to a changing nonradiative decay rate with temperature. This harkens to the assertion of a strong sensitivity of the surface of the Bi-shelled PbS QDs to the quality of passivation, as seen in several studies with other passivating ligands, and implies that there is still much room for further development of these Bi-perovskite shelled QD solids.

## CONCLUSION

We report herein FET and PL measurements on Bi-shelled PbS inks and solids. Our PL measurements on thin films reveal the presence of sub-band gap radiative states, which become visible at temperatures below  $\sim 100$  K, an observation supported by previous studies on PbS-QDs. Using temperature dependent PL measurements, we obtain quenching temperatures (energies) of 231 K, 89 K, and 136 K for the PbS-OA, PbS-MA<sub>3</sub>BiI<sub>6</sub>, and PbS-MA<sub>3</sub>Bi<sub>2</sub>I<sub>9</sub> samples, respectively. From power-dependent measurements, we show that the PL efficiency of the OA samples is much higher than that of the Bi-shelled ones, which suffer from traps, most likely formed at their surfaces during the phase-transfer ligand exchange process. Nevertheless, the results from electrical measurements on FETs show the successful removal of the native-OA ligands, displaying electron dominated transport with modest mobilities of around  $10^{-3}$  cm<sup>2</sup> [V s]<sup>-1</sup> – comparable to the reported values for epitaxial Pb-based shelled samples. These results improve our understanding of Bi-perovskite shelled PbS QD solids, which are contenders for diverse optoelectronic applications such as absorber layers in solar cells and photodetectors.

## SUPPLEMENTARY MATERIAL

The [supplementary material](#) contains output curves of the studied field effect transistors (FETs), T-dependent PL contour plots of QDs shelled with Pb-based ligands (MAPbI<sub>3</sub> and MA<sub>4</sub>PbI<sub>6</sub>), and temperature and power dependent PL spectra of the Bi-shelled QDS and the reference sample at selected temperatures, as well as a

table containing PL quenching parameters of the reference OA and perovskite-shelled samples.

## ACKNOWLEDGMENTS

The authors would like to thank A. F. Kamp and T. Zaharia for technical support. This work benefitted greatly from discussions with H. H. Fang and H. Duim. This work was also part of the research program of the Netherlands Organisation for Scientific Research (NWO), which funds the “Next Generation Organic Photovoltaics (NG-OPV)” focus group (Program No. 130) participating in the Dutch institute for fundamental energy research (DIFFER).

A part of the work was performed at the Energy Campus Nürnberg and supported via the “Aufbruch Bayern” initiative by the State of Bavaria. S.K. acknowledges the Deutsche Forschungsgemeinschaft (DFG) for a postdoctoral research fellowship (Grant No. 408012143).

## REFERENCES

- O. V. Salata, *J. Nanobiotechnol.* **2**, 3 (2004).
- C. E. Probst, P. Zrazhevskiy, V. Bagalkot, and X. Gao, *Adv. Drug Delivery Rev.* **65**, 703 (2013).
- T. C. Harman, P. J. Taylor, M. P. Walsh, and B. E. Laforge, *Science* **297**, 2229 (2002).
- G. H. Carey, A. L. Abdelhady, Z. Ning, S. M. Thon, O. M. Bakr, and E. H. Sargent, *Chem. Rev.* **115**, 12732 (2015).
- P. Wu, Y. Xu, J. Zhan, Y. Li, H. Xue, and H. Pang, *Small* **14**, 1801479 (2018).
- J. M. Luther, J. Gao, M. T. Lloyd, O. E. Semonin, M. C. Beard, and A. J. Nozik, *Adv. Mater.* **22**, 3704 (2010).
- A. P. Alivisatos, *Science* **271**, 933 (1996).
- H. Fu and S. W. Tsang, *Nanoscale* **4**, 2187 (2012).
- A. T. Fafarman, W. Koh, B. T. Dirin, D. K. Kim, D. Ko, S. J. Oh, X. Ye, V. Doan-Nguyen, M. R. Crump, D. C. Reifsnnyder, C. B. Murray, and C. R. Kagan, *J. Am. Chem. Soc.* **133**, 15753 (2011).
- D. V. Talapin and C. B. Murray, *Science* **310**, 86 (2005).
- G. Konstantatos, I. Howard, A. Fischer, S. Hoogland, J. Clifford, E. Klem, L. Levina, and E. H. Sargent, *Nature* **442**, 180 (2006).
- D. Yu, C. Wang, and P. Guyot-Sionnest, *Science* **300**, 1277 (2003).
- E. J. D. Klem, D. D. Macneil, P. W. Cyr, L. Levina, and E. H. Sargent, *Appl. Phys. Lett.* **90**, 183113 (2008).
- D. N. Dirin, S. Dreyfuss, M. I. Bodnarchuk, G. Nedelcu, P. Papagiorgis, G. Itskos, and M. V. Kovalenko, *J. Am. Chem. Soc.* **136**, 6550 (2014).
- M. Liu, O. Voznyy, R. Sabatini, F. P. G. De Arquer, R. Munir, A. H. Balawi, X. Lan, F. Fan, G. Walters, A. R. Kirmani, S. Hoogland, F. Laquai, A. Amassian, and E. H. Sargent, *Nat. Mater.* **16**, 258 (2017).
- H. Aqoma, M. Al Mubarak, W. T. Hadmojo, E. Lee, T. Kim, T. K. Ahn, S. Oh, and S. Jang, *Adv. Mater.* **29**, 1605756 (2017).
- Q. Lin, H. J. Yun, W. Liu, H. J. Song, N. S. Makarov, O. Isaienko, T. Nakotte, G. Chen, H. Luo, V. I. Klimov, and J. M. Pietryga, *J. Am. Chem. Soc.* **139**, 6644 (2017).
- D. M. Balazs, N. Rizkia, H.-H. Fang, D. N. Dirin, J. Momand, B. J. Kooi, M. V. Kovalenko, and M. A. Loi, *ACS Appl. Mater. Interfaces* **10**, 5626 (2018).
- H. Zhang, J. Jang, W. Liu, and D. V. Talapin, *ACS Nano* **8**, 7359 (2014).
- Z. Ning, X. Gong, R. Comin, G. Walters, F. Fan, O. Voznyy, E. Yassitepe, A. Buin, S. Hoogland, and E. H. Sargent, *Nature* **523**, 324 (2015).
- R. A. Lalancette, N. Elliott, and I. Bernal, *J. Cryst. Mol. Struct.* **2**, 143 (1972).
- J. G. Contreras, F. W. B. Einstein, M. M. Gilbert, and D. G. Tuck, *Acta Crystallogr., Sect. B: Struct. Crystallogr. Cryst. Chem.* **33**, 1648 (1977).
- M. Lindsjö, A. Fischer, and L. Kloo, *Z. Anorg. Allg. Chem.* **631**, 1497 (2005).
- L. M. Wu, X. T. Wu, and L. Chen, *Coord. Chem. Rev.* **253**, 2787 (2009).
- U. Dasgupta, B. Kundu, and A. J. Pal, *Sol. RRL* **2**, 1800012 (2018).
- M. Leng, Y. Yang, Z. Chen, W. Gao, J. Zhang, G. Niu, D. Li, H. Song, J. Zhang, S. Jin, and J. Tang, *Nano Lett.* **18**, 6076 (2018).
- A. H. Slavney, T. Hu, A. M. Lindenberg, and H. I. Karunadasa, *J. Am. Chem. Soc.* **138**, 2138 (2016).
- J. Niehaus, H.-J. Egelhaaf, K. C. Tam, A. Köck, M. Sytnyk, P. Maisch, S. Langner, W. Heiss, N. A. Killilea, T. Stubhan, C. J. Brabec, T. Rejek, K. Poulsen, A. YousefiAmin, and M. Halik, *ACS Nano* **13**, 2389 (2019).
- N. Killilea, M. Wu, M. Sytnyk, A. A. Yousefi Amin, O. Mashkov, E. Spiecker, and W. Heiss, *Adv. Funct. Mater.* **29**, 1807964 (2019).
- M. Sytnyk, S. Yakunin, W. Schöfberger, R. T. Lechner, M. Burian, L. Ludescher, N. A. Killilea, A. YousefiAmin, D. Kriegner, J. Stangl, H. Groiss, and W. Heiss, *ACS Nano* **11**, 1246 (2017).
- J. Peng, Y. Chen, X. Zhang, A. Dong, and Z. Liang, *Adv. Sci.* **3**, 1500432 (2015).
- Z. Yang, A. Janmohamed, X. Lan, F. P. García De Arquer, O. Voznyy, E. Yassitepe, G. H. Kim, Z. Ning, X. Gong, R. Comin, and E. H. Sargent, *Nano Lett.* **15**, 7539 (2015).
- B.-W. Park, B. Philippe, X. Zhang, H. Rensmo, G. Boschloo, and E. M. J. Johansson, *Adv. Mater.* **27**, 6806 (2015).
- M. Leng, Z. Chen, Y. Yang, Z. Li, K. Zeng, K. Li, G. Niu, Y. He, Q. Zhou, and J. Tang, *Angew. Chem., Int. Ed.* **55**, 15012 (2016).
- M. A. Hines and G. D. Scholes, *Adv. Mater.* **15**, 1844 (2003).
- I. Moreels, K. Lambert, D. Smeets, and D. De Muynck, *ACS Nano* **3**, 3023 (2009).
- T. Takagahara, *Phys. Rev. B* **47**, 4569 (1993).
- K. Szendrei, M. Speirs, W. Gomulya, D. Jarzab, M. Manca, O. V. Mikhnenko, M. Yarema, B. J. Kooi, W. Heiss, and M. A. Loi, *Adv. Funct. Mater.* **22**, 1598 (2012).
- G. W. Hwang, D. Kim, J. M. Cordero, M. W. B. Wilson, C. H. M. Chuang, J. C. Grossman, and M. G. Bawendi, *Adv. Mater.* **27**, 4481 (2015).
- M. J. Speirs, D. N. Dirin, M. Abdu-Aguye, D. M. Balazs, M. V. Kovalenko, and M. A. Loi, *Energy Environ. Sci.* **9**, 2916 (2016).
- L. Hu, A. Mandelis, Z. Yang, X. Guo, X. Lan, M. Liu, G. Walters, A. Melnikov, and E. H. Sargent, *Sol. Energy Mater. Sol. Cells* **164**, 135 (2017).
- A. G. Shulga, V. Derenskiy, J. M. Salazar-Rios, D. N. Dirin, M. Fritsch, M. V. Kovalenko, U. Scherf, and M. A. Loi, *Adv. Mater.* **29**, 1701764 (2017).
- M. I. Nugraha, S. Kumagai, S. Watanabe, M. Sytnyk, W. Heiss, M. A. Loi, and J. Takeya, *ACS Appl. Mater. Interfaces* **9**, 18039 (2017).
- D. Bederak, D. M. Balazs, N. V. Sukharevska, A. G. Shulga, M. Abdu-Aguye, D. N. Dirin, M. V. Kovalenko, and M. A. Loi, *ACS Appl. Nanomater.* **1**, 6882 (2018).
- D. V. Talapin, J. Lee, M. V. Kovalenko, and E. V. Shevchenko, *Chem. Rev.* **110**, 389 (2010).
- R. Wang, Y. Shang, P. Kanjanaboos, W. Zhou, Z. Ning, and E. H. Sargent, *Energy Environ. Sci.* **9**, 1130 (2016).
- R. D. Schaller, S. A. Crooker, D. A. Bussian, J. M. Pietryga, J. Joo, and V. I. Klimov, *Phys. Rev. Lett.* **105**, 067403 (2010).
- P. J. Roland, K. P. Bhandari, and R. J. Ellingson, *J. Appl. Phys.* **119**, 094307 (2016).
- H. H. Fang, D. M. Balazs, L. Protesescu, M. V. Kovalenko, and M. A. Loi, *J. Phys. Chem. C* **119**, 17480 (2015).
- J. Gao and J. C. Johnson, *ACS Nano* **6**, 3292 (2012).
- C. H. M. Chuang, A. Maurano, R. E. Brandt, G. W. Hwang, J. Jean, T. Buonassisi, V. Bulović, and M. G. Bawendi, *Nano Lett.* **15**, 3286 (2015).
- S. Kahmann, M. Sytnyk, N. Schrenker, G. J. Matt, E. Spiecker, W. Heiss, C. J. Brabec, and M. A. Loi, *Adv. Electron. Mater.* **4**, 1700348 (2018).
- C. Giansante and I. Infante, *J. Phys. Chem. Lett.* **8**, 5209 (2017).
- S. Jin, Y. Zheng, and A. Li, *J. Appl. Phys.* **82**, 3870 (1997).
- M. S. Gaponenko, A. A. Lutich, N. A. Tolstik, A. A. Onushchenko, A. M. Malyarevich, E. P. Petrov, and K. V. Yumashev, *Phys. Rev. B* **82**, 125320 (2010).